ADVANCED MATERIALS
www.advmat.de

The Role of Demixing and Crystallization Kinetics on the Stability of Non-Fullerene Organic Solar Cells

Huawei Hu, Masoud Ghasemi, Zhengxing Peng, Jianquan Zhang, Jeromy James Rech, Wei You, He Yan, and Harald Ade**

With power conversion efficiency now over 17%, a long operational lifetime is essential for the successful application of organic solar cells. However, most non-fullerene acceptors can crystallize and destroy devices, yet the fundamental underlying thermodynamic and kinetic aspects of acceptor crystallization have received limited attention. Here, room-temperature (RT) diffusion coefficients of 3.4×10^{-23} and 2.0×10^{-22} are measured for ITIC-2Cl and ITIC-2F, two state-of-the-art non-fullerene acceptors. The low coefficients are enough to provide for kinetic stabilization of the morphology against demixing at RT. Additionally profound differences in crystallization characteristics are discovered between ITIC-2F and ITIC-2Cl. The differences as observed by secondary-ion mass spectrometry, differential scanning calorimetry (DSC), grazing-incidence wide-angle X-ray scattering, and microscopy can be related directly to device degradation and are attributed to the significantly different nucleation and growth rates, with a difference in the growth rate of a factor of 12 at RT. ITIC-4F and ITIC-4Cl exhibit similar characteristics. The results reveal the importance of diffusion coefficients and melting enthalpies in controlling the growth rates, and that differences in halogenation can drastically change crystallization kinetics and device stability. It is furthermore delineated how low nucleation density and large growth rates can be inferred from DSC and microscopy experiments which could be used to guide molecular design for stability.

Organic solar cells (OSCs) are one of the most promising cost-effective technologies for utilizing solar energy with a short energy payback time and in semi-transparent applications.[1–3] Bulk heterojunction OSCs comprising a donor and acceptor blend as the photoactive layer have achieved impressive improvements in power conversion efficiencies (PCEs) over the past 25 years.[4–7] Owing to the rapid development of high-performance non-fullerene small molecular acceptors (SMAs), PCE of over 15–17% has been achieved in various systems.[8–12] These promising results make non-fullerene OSCs competitive with other types of next-generation solar technology. Among start-of-the-art non-fullerene SMAs, the fused-ring electron acceptor named ITIC, comprising a indacenodithieno[3,2-b]-thiophene core and 2-(3-oxo-2,3-dihydroinden-1-ylidene)malononitrile end-groups, represents the most extensively studied SMA that achieved high performance with various donor polymers.[13–15] A family of high-performance ITIC derivatives was then designed and synthesized to modify the energy levels, light absorption, and molecular packing of the materials, as well as the morphology of the devices, which significantly boosted the performance of non-fullerene OSCs.[16–18] Generally, design rules for modifying energy levels and optical properties exist, but design rules for miscibility and stability are largely missing,[19–22] yet they are of vital importance to guarantee a long operational lifetime. While some conceptual understanding exists that stability must be related to the glass transition of the SMA and the polymer,[19,23–25] the relation of molecular design to the glass transition and crystallization, in general, is unknown and complex, due in part to the complex amphiphilic nature of the materials.

One of the most widely used chemical modification approaches to modulate non-fullerene SMA characteristics is the introduction of electron-withdrawing halogen atoms, which has generated a number of high-performance acceptors.[26,27] Given that fluorine has the highest electronegativity, fluorination can effectively modify the highest occupied molecular orbital of organic semiconductors without introducing undesirable steric hindrance like other, more bulky electron-deficient groups.[28–30]

Dr. H. Hu,[+] Dr. M. Ghasemi, Z. Peng, Prof. H. Ade
Department of Physics and Organic and Carbon Electronics Laboratories (ORaCEL)
North Carolina State University
Raleigh, NC 27695, USA
E-mail: hhuab@connect.ust.hk; hwade@ncsu.edu
Dr. J. Zhang, Prof. H. Yan
Department of Chemistry and Hong Kong Branch of Chinese National Engineering Research Center for Tissue Restoration & Reconstruction
Hong Kong University of Science and Technology (HKUST)
Clear Water Bay, Kowloon, Hong Kong, China
J. J. Rech, Prof. W. You
Department of Chemistry
University of North Carolina at Chapel Hill
Chapel Hill, NC 27599, USA
The ORCID identification number(s) for the author(s) of this article can be found under https://doi.org/10.1002/adma.202005348.
[+]Present address: College of Materials Science and Engineering, Donghua University, Shanghai 201620, China

DOI: 10.1002/adma.202005348

Furthermore, non-covalent intermolecular interactions such as F···H, F···S, and F···π generated from fluorine can exert great influence on the molecular packing of the fluorinated materials in the thin-film devices.[31–33] These unique properties contribute to intensive research activities to exploring fluorination in non-fullerene SMAs, and many excellent fluorinated small molecules such as ITIC-4F,[34] IEICO-4F,[35] IHIC,[36] and Y6[9] have been developed. Chlorination represents another common strategy utilized in adjusting the energy levels and molecular packing of organic semiconductors and achieved many promising results.[37–43] Compared with fluorine, the electronegativity of chlorine is weaker, however, chlorination has a stronger ability in modifying the materials energy levels owing to its empty 3d orbital.[44] Furthermore, the introduction of chlorine could impact molecular packing and thermal properties differently than fluorination due to chlorine's bigger atomic radius. Additionally, it is relatively easier to introduce chlorine into organic semiconductors.[44] These unique proprieties enable a great potential in developing chlorinated high-performance donor or acceptor materials.[45–47]

Although considerable trial-and-error progress has been made with respect to device stability in general, a molecular-level understanding is missing, and a direct comparison of fluorination and chlorination on crystallization instability has rarely been investigated. Generally, the lifetime of a device is controlled by the choice of the photoactive layer and can be affected by several factors, such as oxygen and water, irradiation, mechanical stress, and so on.[24,48,49] Here, we mainly focus on the thermodynamic drivers that govern the morphology instability due to crystallization. It has been shown recently that two major factors dominate the morphological stability:[19,50] i) SMA aggregation/crystallization and depletion of the mixed domain to the liquidus composition, ii) donor–acceptor demixing through binodal/spinodal phase separation. There is a limited indication that other parameters such as molecular orientation or changes in charge transfer docking sites take the leading role in device instability.[51] One example of spinodal demixing is the high-performance PffBT4T-2OD:$PC_{71}BM$ blend system, where quenched domains demix even at room temperature (RT) leading to severe burn-in degradation.[50,52] We surmise that the kinetics of SMA diffusions and crystallization must also greatly influence stability. If sufficiently low, even unstable systems might last for a considerable time.

To elucidate underlying thermodynamic and kinetic properties of SMAs on device stability and simultaneously explore the impact of differences in halogenation, we combine two sets of non-fullerene SMAs including the fluorine-containing acceptors (ITIC-2F and ITIC-4F) and chlorine-containing acceptors (ITIC-2Cl and ITIC-4Cl) with a high-performance wide band-gap donor material FTAZ. FTAZ was deliberately chosen because it is a very ductile, viscoelastic material that generally exhibits poor shelf-life stability with low T_g acceptors.[19,53] It thus allows us to investigate the intrinsic contributions of the small molecule to limitations in stability. Absolute efficiencies achieved are not important in our fundamental study, and the relative PCE is simply used as a proxy for morphology changes. Although FTAZ is ductile, the devices were very stable at RT due to low diffusion coefficients, and accelerated stress tests have been used to infer the relative long-term stability of the systems investigated. The chlorinated devices were more stable than fluorinated devices, which can be mainly attributed to that ITIC-2Cl having a significantly higher crystallization density and lower growth rate than the corresponding ITIC-2F. The high nucleation density of ITIC-2Cl results in many nanocrystals that are not very detrimental, whereas ITIC-2F creates a small number of large crystals that likely short the device. These differences in kinetics can be directly correlated to the smaller melting enthalpy and smaller diffusion coefficient of the chlorinated materials. The result was further confirmed with ITIC-4F and ITIC-4Cl, suggesting that introducing chlorine atoms into SMAs is indeed a generally applicable design to enhance the stability of OSCs. Simple differential scanning calorimetry (DSC) and optical microscopy measurements can be used to screen materials for stability.

We first investigated the thermal stability of FTAZ:ITIC-2Cl and FTAZ:ITIC-2F based devices with an inverted device architecture as depicted in **Figure 1**a. The chemical structures of the polymer donor (FTAZ) and non-fullerene SMAs (ITIC-2F and ITIC-2Cl) used in this work are shown in Figure 1a. The normalized ultraviolet–visible (UV–vis) absorption spectra of the neat materials are shown in Figure 1b. The chlorinated SMA film exhibits a clear red-shifted absorption when compared to the fluorinated counterpart, and both of these two SMAs show complementary absorption with the donor polymer. The current density–voltage (*J*–*V*) and external quantum efficiency (EQE) curves under one sun irradiation of AM1.5G spectrum of the best-performance devices (annealed at 160 °C) are presented in Figure 1c,d, and the averaged performance parameters are summarized in Table S1, Supporting Information. Overall, the as-cast FTAZ:ITIC-2F and FTAZ:ITIC-2Cl devices give a comparable efficiency of 7.5%. The best efficiencies of 9.5% and 9.6% are achieved for FTAZ:ITIC-2F and FTAZ:ITIC-2Cl, respectively, with the devices annealed at 160 °C (close to the T_g of the NFAs, a common optimization condition).[12] It is noted that the relatively low absorption at wavelength below 400 nm of non-fullerene OSC can deliver an EQE about 30%, which has been observed in other reports and is likely due to the efficient exciton dissociation and charge collection and absorption of 40–50% of the incident photons in actual devices.[54] The short-circuit current density (J_{SC}) estimated from EQE is 16.7 and 17.9 mA cm^{-2} for 160 °C annealed FTAZ:ITIC-2F and FTAZ:ITIC-2Cl devices, respectively, which are in a good agreement with the obtained *J*sc from *J*–*V* curves. The open-circuit voltage (V_{OC}) increases after thermal annealed at evaluated temperatures, which is probably due to the increased built-in potential and reduced recombination that increases the current density in the device and the electrochemical potential of the charges.[55] In contrast, aggressive annealing will create crystals that will reduce V_{OC}.[19] It is noted that as the annealing temperature passes 160 °C, the FTAZ:ITIC-2F based device experiences a dramatic decrease in device performance. An efficiency loss of ≈20% and ≈60% are observed upon thermally annealing at 180 and 200 °C for a short period of 10 min (**Figure 2**a), respectively. The PCE loss is a result of decreases in all three photovoltaic parameters, indicating a distinct phase organization and catastrophic failure at such high annealing temperatures.[56] In contrast, the FTAZ:ITIC-2Cl based solar cells do not show an obvious device performance degradation upon thermally annealing at 180 °C,

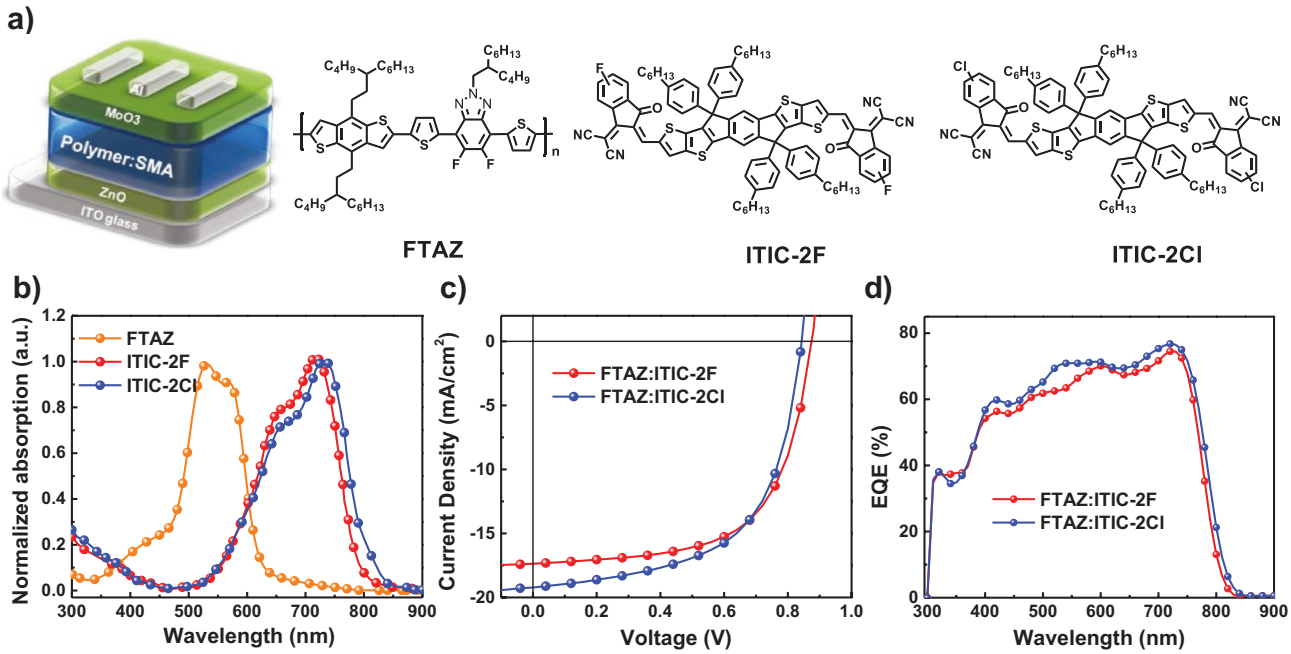

Figure 1. a) Schematic diagram of device structure and chemical structures of FTAZ, ITIC-2F, and ITIC-2Cl as used in this work. b) Normalized UV–vis absorption spectra and of these three materials in thin-film. c,d) Current density versus voltage characteristics and EQE of the OSCs based on FTAZ:ITIC-2F and FTAZ:ITIC-2F annealed at 160 °C for 10 min.

and the PCE loss is only 15% after annealing at 200 °C for 10 min. Further annealing at 220 °C leads to a PCE drop of 84% and 30% for FTAZ:ITIC-2F and FTAZ:ITIC-2Cl based devices, respectively. These results demonstrate that FTAZ:ITIC-2Cl based solar cells exhibit greater thermal stability compared to the corresponding FTAZ:ITIC-2F based devices.

Next, the devices were stored in the dark under N_2 atmosphere for device shelf-life stability testing. Normalized PCE of the devices versus time is shown in Figure 2b and Table S2, Supporting Information. Here, we only compare the shelf-life stability of the as-cast solar cells and devices annealed at 160 °C, which give the best performance. Figure 2b exhibits that both FTAZ:ITIC-2Cl and FTAZ:ITIC-2F based solar cells show excellent shelf-life stability. Specifically, the efficiency of the as-cast and 160 °C annealed FTAZ:ITIC-2Cl and FTAZ:ITIC-2F based solar cells only decreased by less than 2% and 5%, respectively, after 1000 h. The larger efficiency loss in the devices annealed at temperatures of 160 °C comes mainly from losses of J_{SC} and FF, which we attribute to thermally induced crystals of non-fullerene SMA and their growth over time. We note that the relative degradation between as-cast and annealed devices is smaller for ITIC-2Cl than that of ITIC-2F based devices. In the following sections, we will study the major factors (crystallization, demixing, and diffusion coefficients) that governor the morphological stability.

To delineate the reasons behind the observed differences in stability, we first determine the Flory–Huggins interaction

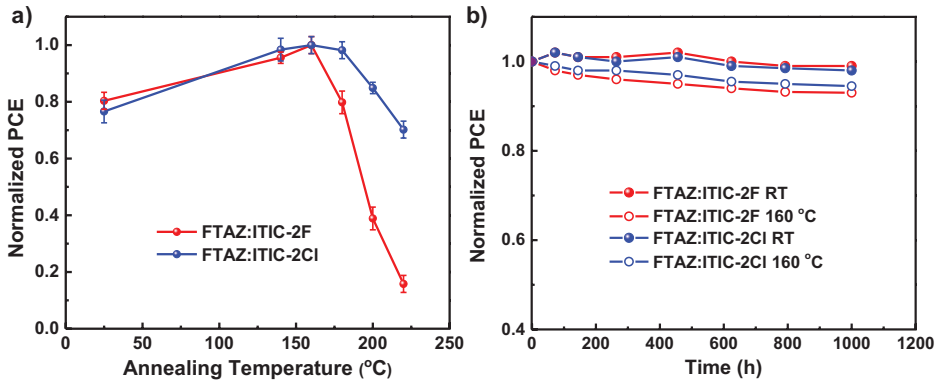

Figure 2. a) Thermal stability behavior of FTAZ:ITIC-2F and FTAZ:ITIC-2F based devices as a function of annealing temperature. Active layers were annealed at each corresponding temperature for 10 min. b) Normalized PCE of non-fullerene SMA based solar cells after long-term storage.

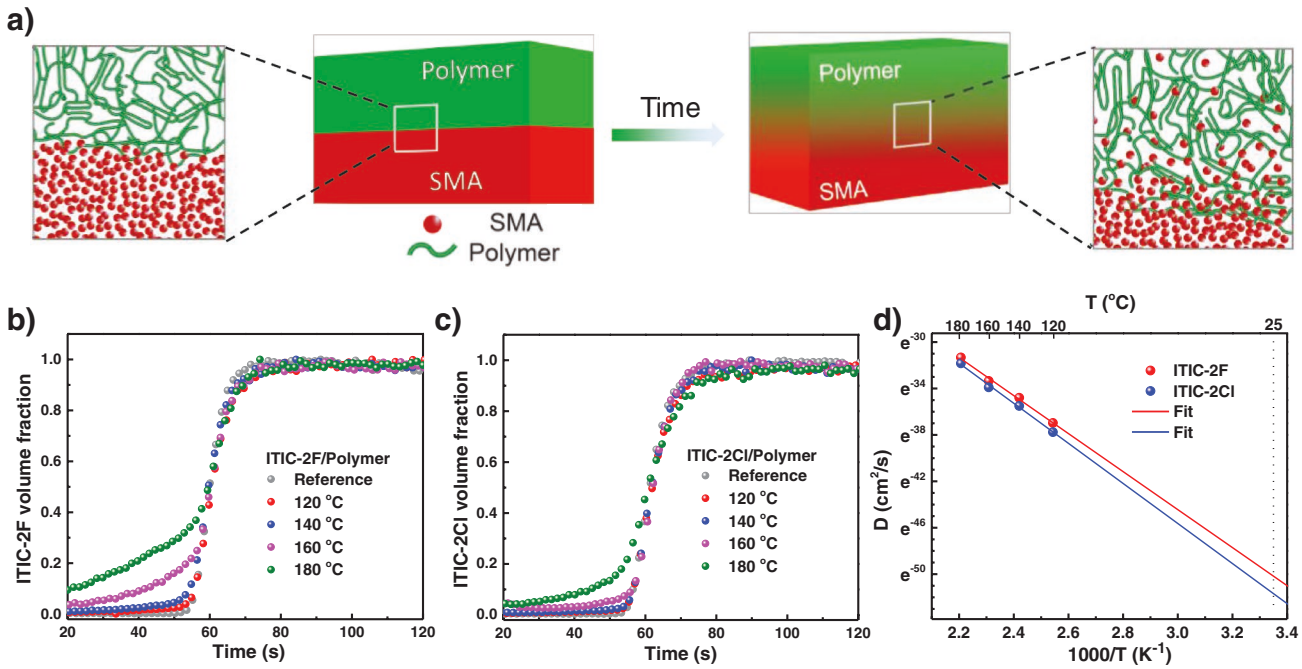

Figure 3. a) Schematic illustration of SIMS diffusion measurements with bilayer structures. b,c) Mass-normalized SIMS profile of bilayers for FTAZ:ITIC-2F and FTAZ:ITIC-2Cl, respectively, annealed at different temperatures. d) Extrapolation of temperature-dependent diffusion coefficients D (T) using fit to Arrhenius equation.

parameter and diffusion coefficients for the fluorinated and chlorinated non-fullerene SMA based systems. Here we use a bilayer interdiffusion experiment[57,58] (**Figure 3**a) that is monitored with time-of-flight secondary-ion mass spectrometry (SIMS) to measure the diffusion coefficients of non-fullerene SMAs into the polymer network. It should be noted here that we use HTAZ, which has the same chemical structures with FTAZ but hydrogen instead of fluorine atoms, as the polymer in all these SIMS measurements (due to similar molecular fragmentation patterns between FTAZ and ITIC-2F, SIMS cannot provide a reliable inter-diffusion data for ITIC-2F into FTAZ). The diffusion concentration profiles $C(x,t)$ at different temperatures T (Figure 3) are fitted using the 1D solution of Fick's second law, $C(x,t) = C(0)\mathrm{erfc}[x/(2\mathrm{sqrt}(\pi Dt)]$, where x is the distance from the interface, t is time, and D is the diffusion coefficient. From the fit of the diffusion concentration profiles (details on the data fitting can be found in the Supporting Information), we can extract the fitting parameter $C(0)$, which corresponds to the equilibrium volume fraction of the non-fullerene SMA in the polymer-rich layer at a certain temperature. The $C(0)$ at 120, 140, 160, and 180 °C are found to be 2.5%, 4.6%, 18.0%, and 31.0%; and 1.8%, 2.6%, 9.0%, and 18.1% for ITIC-2F and ITIC-2Cl based bilayer thin films, respectively. The Flory–Huggins interaction parameter (χ) for polymer:ITIC-2F and polymer:ITIC-2Cl are derived to be $\chi(T) = -10.7 + 5305/T$ and $\chi(T) = -11.2 + 5757/T$, respectively, where T is the absolute temperature. The equilibrium composition of SMA in polymer or $C(0)$ increasing with T is indicative of an upper critical solution temperature phase behavior. Furthermore, a miscibility at RT can be inferred that is well below the assumed percolation threshold of ≈20–30% SMA in the polymer, making both systems an unstable hypo-miscible blend. Given that the differences between HTAZ and FTAZ are subtle and only related to differences in π–π molecular packing but not the interaction with fullerene,[59] we assume that the interaction of the SMAs with FTAZ is similar to that with the HTAZ. The low miscibility provides a strong thermodynamics driver for demixing and over-purification of the mixed domains and thus strong burn-in degradation would be expected as the morphology has to be quenched during casting with a composition of the mixed domains close to or above the percolation threshold.[50,60] However, our results show that both FTAZ:ITIC-2Cl and FTAZ:ITIC-2Cl show excellent shelf-life stability when stored in the dark in a glovebox. This stability should be due to kinetics.

To reveal the reason for the RT stability of FTAZ:ITIC-2F and FTAZ:ITIC-2Cl based solar cells, we extract the diffusion coefficients of these systems from the Fickian fits. As shown from the fits for ITIC-2Cl and ITIC-2F as illustrated in Figure S3, Supporting Information. At 180 °C, these two systems have diffusion coefficients of 1.5×10^{-14} and 2.5×10^{-14} cm^2 s^{-1} for ITIC-2Cl and ITIC-2F, respectively. The slightly larger diffusion coefficient of ITIC-2F suggests that it is likely to be a contributing factor that leads to the difference in thermal stability between ITIC-2Cl and ITIC-2F based devices. By extending the temperature-dependent diffusion coefficients (Figure 3d), we also estimate a D of 3.4×10^{-23} and 2.0×10^{-22} for ITIC-2Cl and ITIC-2F at RT, respectively. This means it would take more than 10 years for these non-fullerene SMA to diffuse 20 nm in the blend film at RT. The very low diffusion coefficients of ITIC-2Cl and ITIC-2F in the donor polymer suggest that the demixing of the mixed-phase that could lead to device burn-in degradation

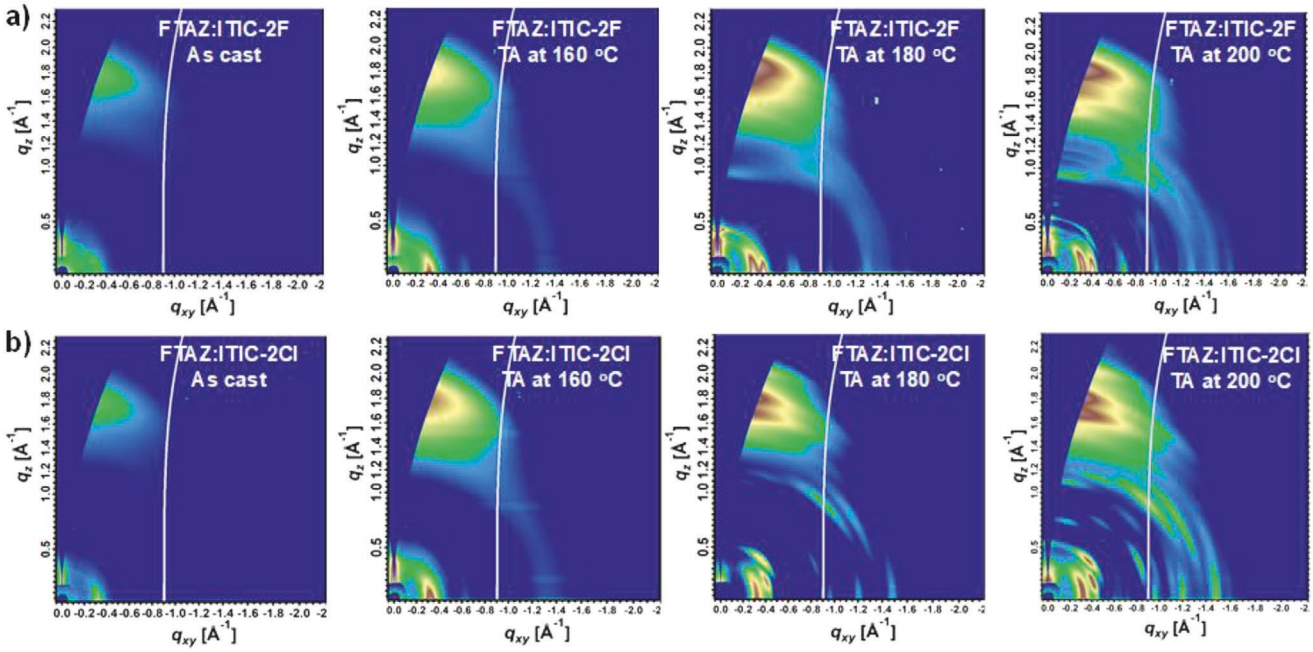

Figure 4. a,b) 2D GIWAXS patterns of FTAZ:ITIC-2F (a) and FTAZ:ITIC-2Cl (b) samples annealed for 10 min at elevated temperatures as indicated. The GIWAXS measurements were done 3 days after the films' preparation annealed. Line cuts and *g*-parameter analysis are provided in the Supporting Information.

is kinetically hindered,[19] which explains the shelf-life stability of solar cells based on these materials.

To reveal a possible origin of the efficiency loss (particularly at high *T*) due to crystallization rather than domain demixing, we performed grazing-incidence wide-angle X-ray scattering (GIWAXS), at beamline 7.3.3[61] of the Advanced Light Source. The 2D patterns of the blend films are shown in **Figure 4**, and the corresponding 1D profile is shown in Figure S1, Supporting Information. From the GIWAXS profiles, the as-cast FTAZ:ITIC-2Cl and FTAZ:ITIC-2F blend films exhibit a well-defined and broad π–π stacking peak in the out-of-plane direction and complementary in-plane (100) peaks for both of the FTAZ and SMAs indicating a face-on preferential orientation relative to the substrates of these materials. It is worth noting that sharp peaks indicative of crystals or aggregates are not observed for all as-cast blend films. However, when the thermal annealing temperature of these blend films is 160 °C, some aggregation signature can be observed for both ITIC-2Cl and ITIC-2F based blends. After thermally annealed at 180 °C, GIWAXS patterns show multiple peaks of the non-fullerene SMA indicative of excellent molecular packing for SMAs annealed at 180 °C. In order to quantitatively analyze the molecular packing, we have analyzed a number of the low q-peaks and calculated the corresponding *g*-parameter, where $g \approx \frac{1}{2\pi}\sqrt{\Delta_q d_h}$, Δ_q and d_h are the full width at half maximum and the interplanar spacing of the diffraction peak of interest, respectively, assuming para-crystallinity as the dominating contribution to the line width. Generally, the smaller *g* indicates the better ordering of the materials.[62,63] Through peak fitting of the 1D GIWAXS profiles of FTAZ:ITIC-2F and FTAZ:ITIC-2Cl based blend films (Figure S2, Supporting Information), we consistently find that that the ITIC-2F has a smaller *g*-parameter than ITIC-2Cl (Table S3, Supporting Information). Specifically, the *g*-parameters at $q = 0.44$ Å^{-1} are found to be 9.6% and 10.5% for 180 °C annealed FTAZ:ITIC-2F and FTAZ:ITIC-Cl based blends, respectively, indicating improved molecular packing of ITIC-2F and possibly larger crystals than that of ITIC-2Cl if the peak width is not dominated by lattice disorder.

It has been widely demonstrated that the formation of crystals of either fullerene or non-fullerene SMA in the blend film would lead to device degradation.[19,64] When considering FTAZ:ITIC-2F, the fast performance degradation of 180 °C compared to 160 °C annealed films can likely be attributed to the presence of highly ordered ITIC-2F SMA crystalline phases in FTAZ:ITIC-2F films annealed at the higher temperature. In contrast, for FTAZ:ITIC-2Cl based devices annealed at 180 °C, no obvious device degradation is observed compared to those solar cells annealed at 160 °C, even though defined peaks are detected in the GIWAXS patterns at 180 °C and there seems to be overall more ordering at 180 °C when compared to the FTAZ:ITIC-2F. The GIWAXS results suggest that the crystallization of the material partially contributes to the device degradation of high temperature (≥180 °C) annealed FTAZ:ITIC-2F samples, while the FTAZ:ITIC-2Cl based devices exhibit excellent thermal stability even though some materials aggregation/crystallization takes place. The contrasting observations between the two SMAs are likely related to the relative size of the crystals, which cannot be easily determined in the presence of lattice disorder, as well as the volume fraction of the crystals. The GIWAXS data is thus inconclusive on its own and we resort below to the use of thermal analysis and microscopy to elucidate crystallization behavior further.

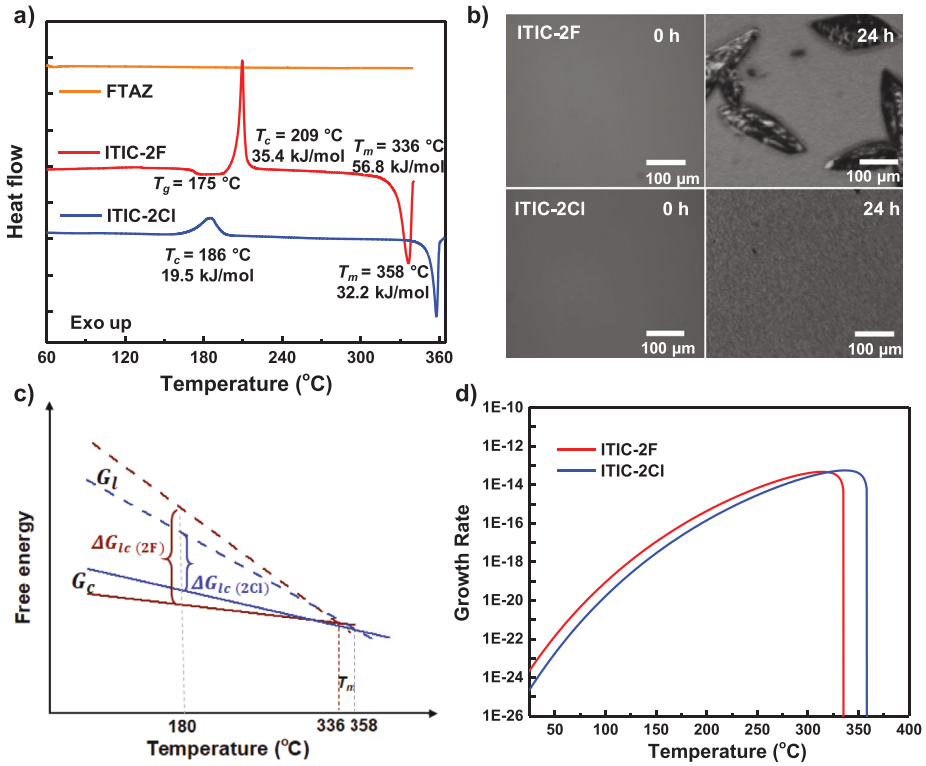

Figure 5. a) DSC thermograms of FTAZ, ITIC-2F, and ITIC-2Cl, collected from the first heat cycle with a 40 °C min^{-1} heating rate. To maximize the crystallization, these materials are processed with solvent vapor annealing for 2 days using chlorobenzene before the DSC measurement. b) Visible light microscopy images of ITIC-2F and ITIC-2Cl after being thermally annealed at 180 °C for 10 min and then using solvent vapor annealing for a certain time as indicated, respectively. c) Schematic illustration of Gibbs free energy of the liquid and crystalline state, G_l and G_C, and the difference in Gibbs free energy as a function of T given the heat of fusion of the ITIC-2F (red) and ITIC-2Cl (blue). d) Temperature-dependent crystallization growth rate defined by growth rate = $D_0(T) \times \exp\left(-\frac{E_A}{kT}\right) \times \left[1-\exp\left(-\frac{\Delta G_{lc}}{kT}\right)\right]$.

To better understand the differences in thermal stability between ITIC-2F and ITIC-2Cl based devices, the thermal proprieties of the neat polymers and non-fullerene SMAs are investigated by DSC. From the DSC data (**Figure 5**a), the donor polymer FTAZ does not show any clear transition peaks, which can be attributed to its amorphous or disordered nature. In contrast, ITIC-2F and ITIC-2Cl exhibit pronounced exothermal peaks (cold crystallization, T_c) at 209 and 186 °C, respectively, suggesting the amorphous volume fraction of these materials starts to reorganize at these temperatures.[65] Additionally, ITIC-2F and ITIC-2Cl also exhibit a well-defined melting peak (T_m) at 336 and 358 °C, with the enthalpies of fusion of 56.8 and 32.2 kJ mol^{-1}, respectively. The observed higher T_m of ITIC-2Cl than ITIC-2F should be attributable to the larger dipole moment of carbon-chlorine bond than the carbon—fluorine bond. The cold crystallization enthalpies of 35.4 and 19.5 kJ mol^{-1} are large fractions of the melting enthalpies, suggesting that the majority of the SMAs are disordered even when the samples are drop cast even as the non-fullerene SMAs have more time to order when compared to spin-coating. Importantly, the T_c peak of ITIC-2F is narrower than that of ITIC-2Cl, and one of the narrowest T_c peaks observed so far. Furthermore, ITIC-2F exhibits a glass transition (T_g) at about 175 °C and the T_c of ITIC-2F is considerately above its T_g. In contrast, ITIC-2Cl does not exhibit the same thermodynamic properties. Instead, the cold crystallization is likely at or just above the T_g and obscures the observation of a glass transition. The difference in width and location of the cold crystallization with respect to the T_g is likely related to the nucleation rate and crystallization kinetics.

To confirm differences in the relative crystallization behavior and nucleation density of ITIC-2F and ITIC-2Cl, we acquired visible light microscope (VLM) images of these two materials. We first anneal the films at 180 °C to create crystals as indicated by GIWAXS and then use solvent vapor annealing (SVA) to assist the further crystallization of these materials by increasing the diffusion coefficient. We note that SVA by itself does not introduce crystals, but simply amplifies the presence of small crystals by furthering their growth. In this way, the observation allows inferences about the nucleation density at 180 °C. The VLM images (Figure 5b) exhibits a few large size (>100 μm) crystals for ITIC-2F based thin film, while only numerous small crystals with size near the optical detection limit can be observed for ITIC-2Cl based film. Again, large differences in crystallization characteristics are observed between the two SMAs.

When considering the GIWAXS, DSC, and VLM data, a self-consistent picture emerges. ITIC-2F has a much lower nucleation rate and density than ITIC-2Cl. The latter rapidly forms

many small, local aggregates or crystals of variable size near its T_g, leading to a broad T_c peak at low T. These nanocrystals can be readily observed by GIWAXS. In contrast, due to just a few nucleation sites in ITIC-2F, significant growth is required before ITIC-2F crystallization can be detected in GIWAXS and DSC. This growth requires large distances and can only occur when there is significant diffusion, a condition that only happens well above the T_g of ITIC-2F. The nucleation of ITIC-2Cl results in a high nucleation density and in many nanocrystals that are not very detrimental to performance, whereas ITIC-2F creates a small number of large crystals that are very detrimental to performance, likely creating shunt-pathways in the devices.[66] For the nanocrystals to lead to shunting failure, they have to grow by Ostwald ripening, which is a very slow process as the chemical potentials of the various crystals are not very different.

In order to establish a relation between crystallization and the differences in melting enthalpy and diffusion coefficients, we consider the crystallization theory of a single material. We note that quantitative measurement of the overall crystallization rate of these non-fullerene SMA requires complex modeling and characterizing that is outside the scope of the current work, but insightful and novel inferences can be made nonetheless. The rate of nucleation and growth of a crystal is given by the following equations:[67,68]

$$\text{Nucleation rate} \propto D(T) \times \exp\left(\frac{-16\pi\gamma_{lc}^3}{3kT\Delta G_{lc}^2}\right) \tag{1}$$

$$\text{Growth rate} \propto D(T) \times \left[1-\exp\left(-\frac{\Delta G_{lc}}{kT}\right)\right] \tag{2}$$

where $D(T)$ is the diffusion coefficient, γ_{lc} is the interfacial energy associated with the surface of the nucleus and ΔG_{lc} is the difference in free energies of liquid and crystalline states (Figure 5c). The latter can be expressed by Equation (3):

$$\Delta G_{lc} = \Delta H_m \times \frac{T_m - T}{T_m} = \Delta H_m \left(1 - \frac{T}{T_m}\right) \tag{3}$$

where ΔH_m is the enthalpy of fusion, and T_m is the melting temperature. Based on the DSC data, the ΔG_{lc} for ITIC-2F and ITIC-2Cl is calculated to be 14.5 and 9.1 kJ mol^{-1} at the temperature of 180 °C, respectively, as an example. Unfortunately, we do not know γ_{lc} and quantitative predictions of the growth to nucleation rates or between the nucleation rates are impossible. We can, however, conclude the growth rate of ITIC-2F and ITIC-2Cl based on Equation (2), and that the growth rate of ITIC-2F is larger than that of ITIC-2Cl by a factor of 3 at 180 °C, and the difference increases with the decreasing temperature to a factor of 12 at RT (Figure 5d). This is largely driven by the differences in diffusion coefficients. We can also infer that the interfacial energy of ITIC-2F is likely larger than that of ITIC-2Cl in order to account for the large differences in nucleation density observed. Irrespective of the limited knowledge of these details, Equations (1) and (3) translate the differences between nucleation rate observed at 180 °C to RT, where the differences in nucleation rates are generally smaller and crystal grow rates are likely dominating. Consequently, ITIC-2F devices are expected to be more prone to crystallization failure than ITIC-2Cl devices at operating temperatures, underscoring, and validating the utility of accelerated thermal stress testing and knowledge of thermal and diffusion characteristics.

To test the generality that chlorinated non-fullerene SMAs give better performance under thermal stress, we investigate the devices based on FTAZ:ITIC-4F and FTAZ:ITIC-4Cl. The device performance under different annealing temperatures are summarized in Table S4, Supporting Information, it can be seen that in the case of ITIC-4Cl, similar to ITIC-2Cl, chlorination of SMA exhibit better thermal stability. The large device degradation (>50% drop of PCE) of FTAZ:ITIC-4F under higher thermal stress mainly comes from the loss of all of the photovoltaic parameters, suggesting the materials strongly crystallized in the blend films, which is evidenced by the GIWAXS patterns (Figure S4, Supporting Information). On the other hand, solar cells based on FTAZ:ITIC-4Cl give a PCE of 7.7% when annealed at 160 °C, which is comparable to that of ITIC-4F based devices processed under the same condition. While the PCEs increase when the annealing temperature was increased to 180 °C even though the crystallization of ITIC-4Cl is detected (Figure S4, Supporting Information), and then slightly decrease after further increasing the annealing temperature. DSC (Figure S5, Supporting Information) of ITIC-4F shows two endothermic peaks (probably due to polymorphism) at 129 and 330 °C with the enthalpy of fusion of 66.0 and 60.0 kJ mol^{-1}, respectively. However, ITIC-4Cl only gives one endothermic peak at 174 °C with a low enthalpy of fusion (15.7 kJ mol^{-1}) with likely sublimation at high temperature or a T_m above the degradation temperature. The results suggest, in complete analogy to the ITIC-2F and ITIC-2Cl comparison, that the growth rate of ITIC-4F as predicted by the difference in free energy ΔG_{lc} should be significantly higher than that of ITIC-4Cl and that the nucleation density of ITIC-4F is much lower. This is confirmed by VLM images (Figure S6, Supporting Information) that ITIC-4F exhibits larger size crystals than that of ITIC-4Cl based thin film. These encouraging results suggest that the introduction of chlorine atoms into non-fullerene acceptors can achieve a much more stable performance than modification of the molecular by fluorination, owing to the significantly lowered melting enthalpy. Importantly, DSC and optical microscopy can be used to infer relative crystallization characteristics and thus long-term device stability.

Overall, the propensity to suffer long term failure due to large crystals penetrating the film has been inferred. The GIWAXS, diffusion, DSC, and SVA annealing measurements reveal a consistent picture that shows that ITIC-2F has a lower nucleation rate compared to ITIC-2Cl, yet higher growth rate due to higher diffusion coefficient that is leading to fewer, larger, and more ordered crystals. This implies that if there are any crystals of ITIC-2F as a result of the film processing protocol, ITIC-2F would more rapidly lead to large crystals that destroy the devices. In contrast, ITIC-2Cl forms numerous nanocrystals with only minimal impact on devices. Similar observations have been made for ITIC-4F and ITIC-4Cl, respectively. The design considerations for non-fullerene SMA synthesis designed to avoid device degradation due to crystallization would thus be: 1) Use of materials with low melting enthalpy, 2) use of materials

with the interfacial energy γ_{lc} as small as possible, and 3) use materials with low diffusion coefficients. While molecular design guidelines should be developed before synthesis commences, our results indicate that the parameters that control device stability are melting enthalpy, glass transition temperature, and melting temperatures, and interfacial energies and that at least the melting enthalpy and melting temperature can be readily checked with DSC post-synthesis. A suitable method to directly measure interfacial energies of crystal nuclei would still have to be found. In the meantime, the impact of interfacial energy has to be inferred from the difference between T_c and T_g in DSC measurements or by the observation of the crystal density with microscopy. In terms of fabrication strategy, it is likely beneficial if a high density of small aggregates can be induced that prevent large crystal formation as is the case for the FTAZ:ITIC-2Cl devices optimized at 160 °C. Given that chlorine is heavier and bulkier than fluorine, there is likely a systematic relation of chemical structure to the relevant thermodynamic quantities. However, melting enthalpy, melting temperatures, and interfacial energy are often difficult to predict in general, not just for semiconducting materials. Fortunately, molecular dynamics simulations are becoming increasingly sophisticated and should be able to assess at least relative characteristics. In the absence of sophisticated simulations before synthesis, our results indicate that determining T_g, T_c, T_m, and ΔH_m can predict relative crystallization characteristics and device stability that can be confirmed through direct observation of the nucleation density.

In summary, through a systematical study of the device performance based on fluorinated or chlorinated ITIC, it is found that the introduction of chlorine atoms into the small molecule electron acceptors appears to be an effective strategy to obtain a device with better operational stability. Furthermore, considering the relatively low cost in synthesizing the chlorinated materials compared with their fluorinated counterparts, chlorinated organic semiconductors have a bright future in the development of OSCs. By revealing the molecular interaction parameter, crystallization, and diffusion coefficients, our research here demonstrates explicitly that a hypomiscible system can still be stable as long as the diffusion coefficients and crystallization rates can be kept sufficiently low. More importantly, our results demonstrate that the crystallization characteristics as revealed by the difference diffusion properties and in Gibbs free energy between liquid and solid phase and the nucleation density as revealed indirectly by a difference between the glass transition and recrystallization temperature can explain and qualitatively predict the operational stability of crystallizable non-fullerene SMA based solar cells. These proxy metrics accessible with DSC measurements and optical microscopy of crystallization characteristics should be able to predict stability beyond the time frame that is readily testable in the research laboratory at RT (even when SIMS measurements are not available) and supports the use of accelerated stress tests.

Supporting Information

Supporting Information is available from the Wiley Online Library or from the author.

Acknowledgements

The research at NCSU by the Ade group was carried out with support from NSF grant CBET-1639429 and ONR grant N000141712204. J.Z. and H.Y. were supported by Shen Zhen Technology and Innovation Commission (JCYJ20170413173814007, JCYJ20170818113905024) W.Y. and J.J.R. were supported by an NSF grant (CBET-1639429). X-ray data were acquired at beamline 7.3.3 at the Advanced Light Source, which is supported by the Director, Office of Science, Office of Basic Energy Sciences, of the U.S. Department of Energy under Contract No. DE-AC02-05CH11231. C. Zhu and A. Hexemer of the ALS (LBNL) provided instrument maintenance. SIMS was performed at the Analytical Instrumentation Facility (AIF) at NCSU, which is partially supported by the State of North Carolina and NSF. The DSC instrument was purchased with UNCGA ROI funds. The authors appreciate Dr. Abay Dinku for maintaining and operating the shared ORaCEL device fabrication facilities at NCSU.

Conflict of Interest

The authors declare no conflict of interest.

Keywords

crystallization kinetics, morphology stability, non-fullerene acceptors, organic solar cells

Received: August 7, 2020
Revised: September 27, 2020
Published online: November 5, 2020

[1] E. Ravishankar, R. E. Booth, C. Saravitz, H. Sederoff, H. W. Ade, B. T. O'Connor, *Joule* **2020**, *4*, 490.
[2] Y. Zhang, S. W. Ng, X. Lu, Z. Zheng, *Chem. Rev.* **2020**, *120*, 2049.
[3] N. Espinosa, M. Hösel, D. Angmo, F. C. Krebs, *Energy Environ. Sci.* **2012**, *5*, 5117.
[4] Y. Huang, E. J. Kramer, A. J. Heeger, G. C. Bazan, *Chem. Rev.* **2014**, *114*, 7006.
[5] G. Yu, J. Gao, J. C. Hummelen, F. Wudl, A. J. Heeger, *Science* **1995**, *270*, 1789.
[6] C. J. Brabec, S. Gowrisanker, J. J. Halls, D. Laird, S. Jia, S. P. Williams, *Adv. Mater.* **2010**, *22*, 3839.
[7] Y. Li, *Acc. Chem. Res.* **2012**, *45*, 723.
[8] S. Liu, J. Yuan, W. Deng, M. Luo, Y. Xie, Q. Liang, Y. Zou, Z. He, H. Wu, Y. Cao, *Nat. Photonics* **2020**, *14*, 300.
[9] J. Yuan, Y. Zhang, L. Zhou, G. Zhang, H.-L. Yip, T.-K. Lau, X. Lu, C. Zhu, H. Peng, P. A. Johnson, M. Leclerc, Y. Cao, J. Ulanski, Y. Li, Y. Zou, *Joule* **2019**, *3*, 1140.
[10] S. Li, C.-Z. Li, M. Shi, H. Chen, *ACS Energy Lett.* **2020**, *5*, 1554.
[11] K. Jiang, Q. Wei, J. Y. L. Lai, Z. Peng, H. K. Kim, J. Yuan, L. Ye, H. Ade, Y. Zou, H. Yan, *Joule* **2019**, *3*, 3020.
[12] Y. Qin, Y. Xu, Z. Peng, J. Hou, H. Ade, *Adv. Funct. Mater.* **2020**, *30*, 2005011.
[13] Y. Lin, J. Wang, Z. G. Zhang, H. Bai, Y. Li, D. Zhu, X. Zhan, *Adv. Mater.* **2015**, *27*, 1170.
[14] Y. Lin, F. Zhao, Q. He, L. Huo, Y. Wu, T. C. Parker, W. Ma, Y. Sun, C. Wang, D. Zhu, A. J. Heeger, S. R. Marder, X. Zhan, *J. Am. Chem. Soc.* **2016**, *138*, 4955.
[15] S. Zhang, Y. Qin, J. Zhu, J. Hou, *Adv. Mater.* **2018**, *30*, 1800868.
[16] Z. Fei, F. D. Eisner, X. Jiao, M. Azzouzi, J. A. Röhr, Y. Han, M. Shahid, A. S. R. Chesman, C. D. Easton, C. R. McNeill, T. D. Anthopoulos, J. Nelson, M. Heeney, *Adv. Mater.* **2018**, *30*, 1705209.

[17] S. Li, L. Zhan, F. Liu, J. Ren, M. Shi, C. Z. Li, T. P. Russell, H. Chen, *Adv. Mater.* **2018**, *30*, 1705208.
[18] J. Sun, X. Ma, Z. Zhang, J. Yu, J. Zhou, X. Yin, L. Yang, R. Geng, R. Zhu, F. Zhang, W. Tang, *Adv. Mater.* **2018**, *30*, 1707150.
[19] M. Ghasemi, H. Hu, Z. Peng, J. J. Rech, I. Angunawela, J. H. Carpenter, S. J. Stuard, A. Wadsworth, I. McCulloch, W. You, H. Ade, *Joule* **2019**, *3*, 1328.
[20] L. Ye, H. Hu, M. Ghasemi, T. Wang, B. A. Collins, J. H. Kim, K. Jiang, J. H. Carpenter, H. Li, Z. Li, T. McAfee, J. Zhao, X. Chen, J. L. Y. Lai, T. Ma, J. L. Bredas, H. Yan, H. Ade, *Nat. Mater.* **2018**, *17*, 253.
[21] H. Hu, L. Ye, M. Ghasemi, N. Balar, J. J. Rech, S. J. Stuard, W. You, B. T. O'Connor, H. Ade, *Adv. Mater.* **2019**, *31*, 1808279.
[22] Y. Zhu, A. Gadisa, Z. Peng, M. Ghasemi, L. Ye, Z. Xu, S. Zhao, H. Ade, *Adv. Energy Mater.* **2019**, *9*, 1900376.
[23] L. Yu, D. Qian, S. Marina, F. A. A. Nugroho, A. Sharma, S. Hultmark, A. I. Hofmann, R. Kroon, J. Benduhn, D. M. Smilgies, K. Vandewal, M. R. Andersson, C. Langhammer, J. Martin, F. Gao, C. Muller, *ACS Appl. Mater. Interfaces* **2019**, *11*, 21766.
[24] J. Xin, X. Meng, X. Xu, Q. Zhu, H. B. Naveed, W. Ma, *Matter* **2019**, *1*, 1316.
[25] C. Müller, *Chem. Mater.* **2015**, *27*, 2740.
[26] C. Yan, S. Barlow, Z. Wang, H. Yan, A. K. Y. Jen, S. R. Marder, X. Zhan, *Nat. Rev. Mater.* **2018**, *3*, 18003.
[27] J. Hou, O. Inganas, R. H. Friend, F. Gao, *Nat. Mater.* **2018**, *17*, 119.
[28] Q. Zhang, M. A. Kelly, N. Bauer, W. You, *Acc. Chem. Res.* **2017**, *50*, 2401.
[29] G. Zhang, X. Xu, Z. Bi, W. Ma, D. Tang, Y. Li, Q. Peng, *Adv. Funct. Mater.* **2018**, *28*, 1706404.
[30] H. Hu, K. Jiang, J.-H. Kim, G. Yang, Z. Li, T. Ma, G. Lu, Y. Qu, H. Ade, H. Yan, *J. Mater. Chem. A* **2016**, *4*, 5039.
[31] T. L. Nguyen, H. Choi, S. J. Ko, M. A. Uddin, B. Walker, S. Yum, J. E. Jeong, M. H. Yun, T. J. Shin, S. Hwang, J. Y. Kim, H. Y. Woo, *Energy Environ. Sci.* **2014**, *7*, 3040.
[32] Y. Deng, J. Liu, J. Wang, L. Liu, W. Li, H. Tian, X. Zhang, Z. Xie, Y. Geng, F. Wang, *Adv. Mater.* **2014**, *26*, 471.
[33] A. C. Stuart, J. R. Tumbleston, H. Zhou, W. Li, S. Liu, H. Ade, W. You, *J. Am. Chem. Soc.* **2013**, *135*, 1806.
[34] W. Zhao, S. Li, H. Yao, S. Zhang, Y. Zhang, B. Yang, J. Hou, *J. Am. Chem. Soc.* **2017**, *139*, 7148.
[35] X. Song, N. Gasparini, L. Ye, H. Yao, J. Hou, H. Ade, D. Baran, *ACS Energy Lett.* **2018**, *3*, 669.
[36] J. Zhu, Z. Ke, Q. Zhang, J. Wang, S. Dai, Y. Wu, Y. Xu, Y. Lin, W. Ma, W. You, X. Zhan, *Adv. Mater.* **2017**, *29*, 1704713.
[37] H. Lai, H. Chen, J. Zhou, J. Qu, P. Chao, T. Liu, X. Chang, N. Zheng, Z. Xie, F. He, *iScience* **2019**, *17*, 302.
[38] Y. Chen, T. Liu, H. Hu, T. Ma, J. Y. L. Lai, J. Zhang, H. Ade, H. Yan, *Adv. Energy Mater.* **2018**, *8*, 1801203.
[39] Y. Li, J. D. Lin, X. Che, Y. Qu, F. Liu, L. S. Liao, S. R. Forrest, *J. Am. Chem. Soc.* **2017**, *139*, 17114.
[40] J. Zhang, Y. Li, H. Hu, G. Zhang, H. Ade, H. Yan, *Chem. Mater.* **2019**, *31*, 6672.
[41] G. Li, D. Li, R. Ma, T. Liu, Z. Luo, G. Cui, L. Tong, M. Zhang, Z. Wang, F. Liu, L. Xu, H. Yan, B. Tang, *J. Mater. Chem. A* **2020**, *8*, 5927.
[42] J.-L. Wang, K.-K. Liu, L. Hong, G.-Y. Ge, C. Zhang, J. Hou, *ACS Energy Lett.* **2018**, *3*, 2967.
[43] S.-S. Wan, X. Xu, Z. Jiang, J. Yuan, A. Mahmood, G.-Z. Yuan, K.-K. Liu, W. Ma, Q. Peng, J.-L. Wang, *J. Mater. Chem. A* **2020**, *8*, 4856.
[44] Y. Zhang, H. Yao, S. Zhang, Y. Qin, J. Zhang, L. Yang, W. Li, Z. Wei, F. Gao, J. Hou, *Sci. China: Chem.* **2018**, *61*, 1328.
[45] C. Yan, T. Liu, Y. Chen, R. Ma, H. Tang, G. Li, T. Li, Y. Xiao, T. Yang, X. Lu, X. Zhan, H. Yan, G. Li, B. Tang, *Sol. RRL* **2020**, *4*, 1900377.
[46] Y. Cui, H. Yao, J. Zhang, K. Xian, T. Zhang, L. Hong, Y. Wang, Y. Xu, K. Ma, C. An, C. He, Z. Wei, F. Gao, J. Hou, *Adv. Mater.* **2020**, *32*, 1908205.
[47] Q. Zhao, J. Qu, F. He, *Adv. Sci.* **2020**, *7*, 2000509.
[48] W. R. Mateker, M. D. McGehee, *Adv. Mater.* **2017**, *29*, 1603940.
[49] P. Cheng, X. Zhan, *Chem. Soc. Rev.* **2016**, *45*, 2544.
[50] N. Li, J. D. Perea, T. Kassar, M. Richter, T. Heumueller, G. J. Matt, Y. Hou, N. S. Guldal, H. Chen, S. Chen, S. Langner, M. Berlinghof, T. Unruh, C. J. Brabec, *Nat. Commun.* **2017**, *8*, 14541.
[51] X. Jiao, L. Ye, H. Ade, *Adv. Energy Mater.* **2017**, *7*, 1700084.
[52] Y. Liu, J. Zhao, Z. Li, C. Mu, W. Ma, H. Hu, K. Jiang, H. Lin, H. Ade, H. Yan, *Nat. Commun.* **2014**, *5*, 5293.
[53] N. Balar, J. J. Rech, R. Henry, L. Ye, H. Ade, W. You, B. T. O'Connor, *Chem. Mater.* **2019**, *31*, 5124.
[54] L. Ye, Y. Xiong, Q. Zhang, S. Li, C. Wang, Z. Jiang, J. Hou, W. You, H. Ade, *Adv. Mater.* **2018**, *30*, 1705485.
[55] M. Mas-Montoya, J. Li, M. M. Wienk, S. C. J. Meskers, R. A. J. Janssen, *J. Mater. Chem. A* **2018**, *6*, 19520.
[56] M. Jørgensen, K. Norrman, F. C. Krebs, *Sol. Energy Mater. Sol. Cells* **2008**, *92*, 686.
[57] N. D. Treat, A. Varotto, C. J. Takacs, N. Batara, M. Al-Hashimi, M. J. Heeney, A. J. Heeger, F. Wudl, C. J. Hawker, M. L. Chabinyc, *J. Am. Chem. Soc.* **2012**, *134*, 15869.
[58] H. W. Ro, B. Akgun, B. T. O'Connor, M. Hammond, R. J. Kline, C. R. Snyder, S. K. Satija, A. L. Ayzner, M. F. Toney, C. L. Soles, D. M. DeLongchamp, *Macromolecules* **2012**, *45*, 6587.
[59] W. Li, S. Albrecht, L. Yang, S. Roland, J. R. Tumbleston, T. McAfee, L. Yan, M. A. Kelly, H. Ade, D. Neher, W. You, *J. Am. Chem. Soc.* **2014**, *136*, 15566.
[60] L. Ye, B. A. Collins, X. jiao, J. Zhao, H. Yan, H. Ade, *Adv. Energy Mater.* **2018**, *8*, 1703058.
[61] A. Hexemer, W. Bras, J. Glossinger, E. Schaible, E. Gann, R. Kirian, A. MacDowell, M. Church, B. Rude, H. Padmore, *J. Phys.: Conf. Ser.* **2010**, *247*, 012007.
[62] J. Rivnay, R. Noriega, R. J. Kline, A. Salleo, M. F. Toney, *Phys. Rev. B* **2011**, *84*, 045203.
[63] J. A. Bartelt, Z. M. Beiley, E. T. Hoke, W. R. Mateker, J. D. Douglas, B. A. Collins, J. R. Tumbleston, K. R. Graham, A. Amassian, H. Ade, J. M. J. Frechet, M. F. Toney, M. D. McGehee, *Adv. Energy Mater.* **2013**, *3*, 364.
[64] S. Wang, Y. Qu, S. Li, F. Ye, Z. Chen, X. Yang, *Adv. Funct. Mater.* **2015**, *25*, 748.
[65] Y. S. Sun, E. M. Woo, *Polymer* **2001**, *42*, 2241.
[66] C. Lindqvist, J. Bergqvist, C.-C. Feng, S. Gustafsson, O. Bäcke, N. D. Treat, C. Bounioux, P. Henriksson, R. Kroon, E. Wang, A. Sanz-Velasco, P. M. Kristiansen, N. Stingelin, E. Olsson, O. Inganäs, M. R. Andersson, C. Müller, *Adv. Energy Mater.* **2014**, *4*, 1301437.
[67] A. D. de Zerio, C. Müller, *Adv. Energy Mater.* **2018**, *8*, 1702741.
[68] L. Cormier, *Procedia Mater. Sci.* **2014**, *7*, 60.